tary Tables I-V and are deposited.

Acknowledgment. We are grateful to the National Sciences and Engineering Research Council for support of this work. Mr. Hartstock is the holder of an NSERC predoctoral fellowship.

Registry No. 1 (R = CH_3; M = Mo), 69140-73-4; **1** (R = H; M = Mo), 56200-27-2; **1** (R = CH_3; M = W), 92670-32-1; **5** (R = R′ = CH_3; R″ = C_2H_5), 92670-33-2; **5** (R = H; R′ = CH_3; R″ = C_2H_5), 92670-34-3; **5** (R = H; R′ = $PhCH_2$; R″ = p-$CH_3OC_6H_4CH_2$), 92670-35-4; **6** (M = Mo; R = H; R′ = CH_3; R″ = C_2H_5), 92670-36-5; **6**·0.5CH_2Cl_2 (M = Mo; R = H; R′ = CH_3; R″ = C_2H_5), 92760-84-4; **6** (M = Mo; R = R′ = CH_3; R″ = C_2H_5), 92670-38-7; $(CH_3C_5H_4)_2Mo_2(CO)_6$, 33056-03-0; $(C_5H_5)_2Mo_2(CO)_6$, 12091-64-4; $(CH_3C_5H_4)_2W_2(CO)_6$, 68111-11-5; ethyl dithioacetate, 870-73-5; p-methoxybenzyl benzenedithioacetate, 92670-39-8.

Supplementary Material Available: Tables of thermal and hydrogen atom parameters, temperature factors, additional bond lengths and angles, least-squares planes, and structure factors for **5** and **6** (55 pages). Order information is given on any current masthead page.

Electronic Coupling in Delocalized Mixed-Valence Dimers

Lucjan Dubicki, James Ferguson,* and Elmars R. Krausz

Contribution from the Research School of Chemistry, Australian National University, Canberra, A.C.T., 2601, Australia. *Received May 24, 1984*

Abstract: The electronic absorption spectra of the Creutz-Taube mixed-valence ion and its osmium analogue have been reinvestigated, and a simple effective pair model has been developed. This model successfully interprets the anisotropy of the EPR g values and MCD spectra of the Creutz-Taube ion and provides an assignment of the visible and near-IR absorption spectra of the osmium analogue. Indications of further complexities in the Creutz-Taube ion are outlined.

The properties of the mixed-valence decaammine(μ-pyrazine-N,N')diruthenium(5+) (Creutz-Taube) ion have generated considerable debate with regard to its electronic structure, and a recent contribution has summarized and reviewed the evidence for and against a delocalized model.[1] The case for delocalization, based on analyses of the EPR and optical data, has been put by Hush et al.,[2,3] but the optical argument revolves around the width of the near-infrared absorption band, and, so far, no framework has been developed to interpret the polarized spectra of delocalized mixed-valence complex ions. Such a model should also be compatible with the EPR data so that both EPR and optical data can be treated within the same framework. Several attempts to model the system have been made; some concentrate on vibronic effects[4,5] while others work within a molecular orbital description,[6,7] intuitively more appealing from the viewpoint of inorganic chemistry. None of these deals satisfactorily with the polarization of the electronic absorption spectra.

We have found that magnetic circular dichroism (MCD) can be used to great advantage in understanding the near-infrared absorption spectra of many osmium(III) and ruthenium(III) complex ions.[8,9] A similar situation applies to mixed-valence complex ions involving these metals, and we have developed the simplest type of model that can be used to interpret the MCD of these materials. The approach arises naturally from the one we developed to interpret the electronic properties of the $(Ru,Os)^{3+}$ ions which have the t_2^5 configuration. Our model is based on an effective Hamiltonian for the $^2T_2$ term along with a consideration of the effective electric dipole transition moments associated with the odd parity potentials of the ligand field experienced by each metal ion. These potentials break down the Laporte restriction within each metal ion d shell and also provide for two-center excitations between the metal ions. The latter transition dipoles can interfere with the former and provide a net MCD signal when the external magnetic field lies transverse to the direction of the metal ions. This approach uses "transfer integrals" to describe the coupling between the two metal ions and enables a reinterpretation of the existing EPR data as well as the electronic absorption spectrum of the Creutz-Taube ion and the electronic spectrum of the osmium analogue. The present paper deals with these matters while another work[10] reports a corresponding analysis of the properties of the dinitrogen osmium 5+ mixed-valence ion.

Table I. Effective Single-Ion Hamiltonian and Energy Matrix (Units of λ)

$$\mathcal{H}_{eff} = \Delta(L_Z^2 - {}^2/_3) - \beta(L_X^2 - L_Y^2) - \lambda L\cdot S$$

$\pm 1/2X_\pm$	$\Delta/3 + {}^1/_2$	0	$-\beta$
$\mp 1/2X_0$	0	$-2\Delta/3$	$1/2^{1/2}$
$\pm 1/2X_\mp$	$-\beta$	$1/2^{1/2}$	$\Delta/3 - {}^1/_2$

$$|\pm 1/2X_\pm\rangle = |x_\pm^2 \overset{\pm}{x}_\mp x_0^2|$$
$$|\mp 1/2X_0\rangle = -|x_\pm^2 \overset{\mp}{x}_\mp x_0|$$
$$|\pm 1/2X_\mp\rangle = |\overset{\pm}{x}_\pm x_\mp^2 x_0^2|$$

EPR Spectra

The original powder and glass measurements of Bunker et al.[11] were shown to be incomplete by Hush et al.[3] through their single-crystal study. Hush et al.[3] concluded that the Creutz-Taube ion has approximate tetragonal symmetry with the principal axis ($g_\parallel$) perpendicular to the pyrazine ring, not along the Ru-pyr-Ru axis. This accidental or pseudotetragonal description can occur if the tetragonal (Δ) and rhombic (β) field parameters (defined

(1) Fuerholz, U.; Ludi, A.; Buergi, H.-B.; Wagner, F. E.; Stebler, A.; Ammeter, J. H.; Krausz, E. R.; Clark, R. J. H.; Stead, J. *J. Am. Chem. Soc.* **1984**, *106*, 121-123.
(2) Beattie, J. K.; Hush, N. S.; Taylor, P. R. Inorg. *Chem.* **1976**, *15*, 992-993.
(3) Hush, N. S.; Edgar, A.; Beattie, J. K. *Chem. Phys. Lett.* **1980**, *69*, 128-133.
(4) Piepho, S. B.; Krausz, E. R.; Schatz, P. N. *J. Am. Chem. Soc.* **1978**, *100*, 2996-3005.
(5) Schatz, P. N.; Piepho, S. B.; Krausz, E. R. *Chem. Phys. Lett.* **1978**, *55*, 539-542.
(6) Hush, N. S. *Chem. Phys.* **1975**, *10*, 361-366.
(7) Lauher, J. W. *Inorg. Chim. Acta* **1980**, *39*, 119-123.
(8) Dubicki, L.; Ferguson, J.; Krausz, E. R.; Lay, P. A.; Maeder, M.; Taube, H. *J. Phys. Chem.* **1984**, *88*, 3940-3941.
(9) Dubicki, L.; Ferguson, J.; Krausz, E. R.; Lay, P. A.; Maeder, M.; Taube, H., unpulished results.
(10) Dubicki, L.; Ferguson, J.; Krausz, E. R.; Lay, P. A.; Maeder, M.; Magnuson, R. H.; Taube, H., manuscript in preparation.
(11) Bunker, B. C.; Drago, R. S.; Hendrickson, R. M.; Richman, R. M.; Kessell, S. L. *J. Am. Chem. Soc.* **1978**, *100*, 3805-3814.

0002-7863/85/1507-0179$01.50/0

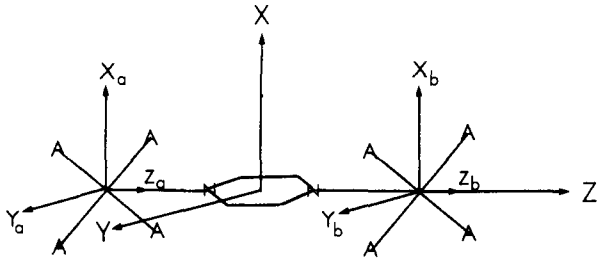

Figure 1. Coordinate axis system for the pair.

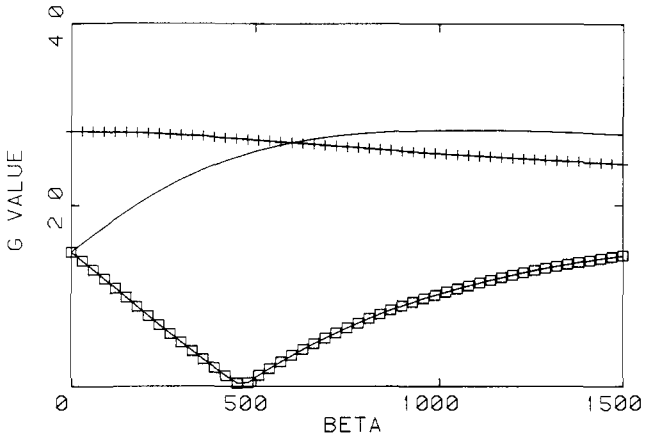

Figure 2. Calculated g_X (□), g_Y (–), and g_Z (+) as a function of β with $\Delta = -600$ cm^{-1} and $\lambda = 1000$ cm^{-1}.

below) have the same magnitude. In such a case, g_X becomes equal to g_Z or g_Y (see Figure 1 for axis convention), dependent on the sign of β. Hush et al.[3] were unable to identify the two components of $g_\perp$. Recent work[1] has provided the complete anisotropy,

$$g_X = 1.346\ (3) \quad g_Y = 2.799\ (3) \quad g_Z = 2.487\ (3)$$

These data can be fitted to within experimental error by using an effective single-ion Hamiltonian with the values $\Delta = -606.5$ cm^{-1}, $\beta = -1340.8$ cm^{-1}, and $\lambda = 1000$ cm^{-1} and an orbital reduction factor of 0.981.

We note that β is more than twice Δ. This arises because the g_X,g_Y anisotropy is only weakly dependent on the rhombic field over a large range, as shown in Figure 2.

The foregoing analysis and that of Hush et al.[3] are both single-ion approaches. There is, of course, nothing wrong with a single-ion approach except that details of the interion interaction are hidden within the overall tetragonal and rhombic field parameters. It is reasonable to introduce the interion interaction explicity as follows in a consideration of the effective Hamiltonian.

Effective Hamiltonian for the Dimer

With reference to Figure 1 we introduce the three t_2 orbitals $\xi'(YZ)$, $\eta'(XZ)$, and ν' $(X^2 - Y^2)$ for Ru in a C_{2v} site. Convenient C_{2v} complex bases are $|x_\pm\rangle = (\eta' \mp i\xi')/2^{1/2}$, $|x_0\rangle = |\nu'\rangle$.

The five-electron effective Hamiltonian for the C_{2v} site is given in Table I along with the energy matrix, where λ is positive and Δ and β are the one-electron tetragonal and rhombic splittings. $\Delta = E(\nu') - E(\xi',\eta')$, and $\beta = E(\xi') - E(\eta')$. This Hamiltonian could be used to consider the energy levels of the complex ion $[(NH_3)_5Os(isonicotinamide)]^{3+}$, for example.[8]

For a delocalized dimer the Hamiltonian is $\mathcal{H} = \mathcal{H}_a + \mathcal{H}_b + \mathcal{H}_{ab}$, where $\mathcal{H}_a$ and $\mathcal{H}_b$ are the single-ion Hamiltonians (Table I) corresponding to the configurations $t_{2a}^5(^2T_2)t_{2b}^6(^1A_1)$ and $t_{2a}^6(^1A_1)t_{2b}^5(^2T_2)$, respectively. The pair interaction, $\mathcal{H}_{ab}$, is taken to be the spin-independent excitation transfer,[12]

$$\langle {}^2T_2M_a\,{}^1A_{1b}|\mathcal{H}_{ab}|{}^1A_{1a}\,{}^2T_2M_b\rangle = -W(M_a,M_b)$$

The number of such transfer integrals (W) is restricted by symmetry, and for a D_{2h} pair, $M_a = m_b = \xi'$, η', and ν'. For the Creutz–Taube ion the most important interaction between the two metal ions should be π-bonding of the η' orbitals with the pyrazine bridge (Figure 1). Therefore we assume that the pair interaction is dominated by

$$\langle \eta'_a|\mathcal{H}_{ab}|\eta'_b\rangle = +W(\eta'_a,\eta'_b) = W$$

The orbitals ξ', η', and ν' are taken to the orthogonalized atomic orbitals, and the transfer integrals are the same as those occurring in the kinetic exchange for coupled pairs of insulator ions.[12]

The pair functions and energy matrices are given in Table II. The pair energy matrices have been given in a form that shows quite clearly their similarity to the single-ion energy matrix (Table I). The effect of W is seen to rescale the single-ion parameters Δ and β. For the Creutz–Taube ion a simple MO picture with strong π-backbonding suggests that the unpaired electron is in b_{2g} MO so that W is positive and the B multiplet is lower. We can now fix W from the energy of the intense band (6200 cm^{-1}), and we then calculate the g factors to within their experimental errors by using $\Delta = 843.8$ cm^{-1} and $\beta = 109.2$ cm^{-1} with $\lambda = 1000$ cm^{-1}, $W = 2900$ cm^{-1}, and the same orbital reduction factor of 0.981. Δ and β are now positive, but the rhombic field β is very small, which is consistent with pyrazine having little π-bonding with the Ru^{3+} for a single-ion complex. The two sets of parameters are simply connected by $-1/2\ W$ (Table II), but the pair analysis reveals the true single-ion parameters, which are similar in magnitude and sign to those obtained from a study of Os(III) complex ion spectra.[8]

Relevant to this point we have repeated some of the EPR measurements of Bunker et al.[11] on frozen solutions and powders. We were able to reproduce their spectra of the Creutz–Taube complex and its oxidized Ru^{3+}–pyr–Ru^{3+} form as well as the (pyrazine)pentaammineruthenium(3+) monomer. Moreover we were able to locate the missing feature at $g = 1.4$ in the Creutz–Taube system by increasing the spectrometer gain. Single-crystal measurements have identified this as g_X. No such feature was discernible in the spectra of the oxidized form or the monomer.

When the pair interaction W is switched off, our values of $\Delta = 843.8$ cm^{-1} and $\beta = 109.2$ cm^{-1} should provide reasonable estimates of the parameters of both the oxidized 6+ ion and the 3+ monomer. The calculated g values are $g_X = 2.74$, $g_y = 2.41$, and $g_Z = 0.29$. This is reasonably consistent with the experimental g of 2.68 and an asymmetric EPR line shape found for both the monomer and oxidized dimer. An oriented single-crystal measurement would be useful as it would also show that the symmetry direction is Z and not X as in the Creutz–Taube ion.

Transition Electric Dipole

Interpretation of the absorption spectra and the MCD of the dimer requires consideration of transition intensity mechanisms. The magnetic dipole process cannot explain the magnitudes of

Table II

Pair Functions[a]

$$\Phi_{1\mp}{}^B = [(d_a{}^6,\pm 1/2X_{b\pm}) + (\pm 1/2X_{a\pm},d_b{}^6)]/2^{1/2}$$
$$\Phi_{2\mp}{}^B = [(d_a{}^6,\mp 1/2X_{b0}) + (\mp 1/2X_{a0},d_b{}^6)]/2^{1/2}$$
$$\Phi_{3\mp}{}^B = [(d_a{}^6,\pm 1/2X_{b\mp}) + (\pm 1/2X_{b\mp},d_b{}^6)]/2^{1/2}$$

Energy Matrices (Units of λ)[b]

$\Phi_{1\pm}{}^B$	$\Delta_B/3 + 1/2$	0	$-\beta_B$		$-W/3$	0	0
$\Phi_{2\mp}{}^B$	0	$-2\Delta_B/3$	$1/2^{1/2}$	+	0	$-W/3$	0
$\Phi_{3\mp}{}^B$	$-\beta_B$	$1/2^{1/2}$	$\Delta_B/3 - 1/2$		0	0	$-W/3$
$\Phi_{1\mp}{}^A$	$\Delta_A/3 + 1/2$	0	$-\beta_A$		$W/3$	0	0
$\Phi_{2\mp}{}^A$	0	$-2\Delta_A/3$	$1/2^{1/2}$	+	0	$W/3$	0
$\Phi_{3\mp}{}^A$	$-\beta_A$	$1/2^{1/2}$	$\Delta_A/3 - 1/2$		0	0	$W/3$

[a] For A functions the + combination is replaced by –. [b] $\Delta_B = \Delta - W/2$; $\Delta_A = \Delta + W/2$; $\beta_B = \beta - W/2$; $\beta_A = \beta + W/2$.

(12) Gondaira, K.; Tanabe, Y. *J. Phys. Soc. Jpn.* **1976**, *21*, 1527–1548.

Table III. Effective Electric Dipole Transition Matrix Elements in Terms of the Reduced Matrix Elements a, b, c, and d[a]

$a = -1/3\langle T_2||V(A_1)||T_2\rangle$; $b = 1/[3(2)^{1/2}]\langle T_2||V(E)||T_2\rangle$; $c = 1/(2/3)^{1/2}\langle T_2||V(T_2)||T_2\rangle$; $d = 1/6^{1/2}\langle T_2||V(T_2)|T_2\rangle$

$\langle \pm 1/2X_0|P^X|\pm 1/2X_\pm\rangle = \langle \mp 1/2X_0|P^X|\mp 1/2X_\pm\rangle = \mp(-c+d)/2^{1/2}$
$\langle \pm 1/2X_0|P^X|\pm 1/2X_\mp\rangle = \langle \mp 1/2X_0|P^X|\mp 1/2X_\mp\rangle = \pm(-c+d)/2^{1/2}$
$\langle \pm 1/2X_0|P^Y|\pm 1/2X_\pm\rangle = \langle \mp 1/2X_0|P^Y|\mp 1/2X_\pm\rangle = i(c+d)/2^{1/2}$
$\langle \pm 1/2X_0|P^Y|\pm 1/2X_\mp\rangle = \langle \mp 1/2X_0|P^Y|\mp 1/2X_\mp\rangle = i(c+d)/2^{1/2}$
$\langle \pm 1/2X_\pm|P^Z|\pm 1/2X_\mp\rangle = \langle \mp 1/2X_\pm|P^Z|\mp 1/2X_\mp\rangle = -d$
$\langle \pm 1/2X_\pm|P^Z|\pm 1/2X_\pm\rangle = \{\mp 1/2X_\pm|P^Z|\mp 1/2X_\pm\rangle = a+b$
$\langle \pm 1/2X_0|P^Z|\pm 1/2X_0\rangle = \langle \mp 1/2X_0|P^Z|\mp 1/2X_0\rangle = a-2b$

[a] The parameters a, b and c are associated with the odd parity tetragonal potential, and d is associated with the rhombic potential. If the matrix elements apply to a hole at center b ($d_a^6d_b^5$ configuration), then the corresponding set for $d_a^5d_b^6$ is equal in magnitude but opposite in sign (see text).

the observed intensities, so we need to develop an electric dipole mechansim. Ignoring energy denominators, we use the approach of Sugano, Tanabe, and Kamimura[13] to obtain effective electric dipole transition moment operators

$$P_{\text{eff}}^{\alpha} \propto V_{\text{odd}}(\Gamma M)P(T_{1u\alpha}) = \sum_{\bar{\Gamma}} V(\bar{\Gamma}\bar{M})\langle \bar{\Gamma}\bar{M}|\Gamma M T_{1\alpha}\rangle$$

There are two odd parity potentials, $V(T_{1uZ})$ (tetragonal) and $V(A_{2ue_2})$ (rhombic). P_{eff}^{α} is represented by the cubic tensors $V(\bar{\Gamma}\bar{M})$, for example,

$$P^Z \propto -1/[3V(A_1e_1)]^{1/2} - 2/[6V(E_{u'})]^{1/2} + V(T_{2v'})$$

where the first two tensors are associated with the tetragonal potential and $V(T_{2v'})$ is associated with the rhombic potential. The real cubic tensor $V(T_1)$ does not contribute to transitions within a Russell–Saunders multiplet.[13] The tensor $V(A_1)$ does not contribute to transitions within a monomer. For a pair, the operator $V(A_1)_a + V(A_1)_b$ effectively represents the Z-polarized electric dipole for the electron transfer, $d_a^6d_b^5 \leftrightarrow d_a^5d_b^6$. Using the complex basis $|SM_ST_2M\rangle = |M_SM\rangle$, then

$$\langle SM_ST_2M|V(\bar{\Gamma}\bar{M})|SM_S'T_2M'\rangle = \delta_{M_SM_S'}\langle T_2||V(\bar{\Gamma})||T_2\rangle\langle T_2M|T_2M'\bar{\Gamma}\bar{M}\rangle/3^{1/2}$$

and the reduced matrix elements are listed in Table III. This table applies to both D_{2h} and D_{4h} pairs, the latter having $d = 0$. The odd parity potentials have opposite phases at the two metal ions. For delocalized D_{4h} or D_{2h} pairs the single-ion transition moments at the two centers are equal and opposite in sign. It is sufficient to use wave functions for a d^5 monomer with Δ and β parameters corresponding to the A and B multiplets. For Z quantization the ground-state wave function has the form

$$\Phi_{0\mp}{}^Z = a_0(\mp 1/2X_0) + b_0(\pm 1/2X_\pm) + c_0(\pm 1/2X_\mp)$$

and is obtained by diagonalization of the $^2T_2$ matrix with the effective parameters Δ_B and β_B. The excited states have the form

$$\Phi_{i\pm}{}^Z = a_i(\pm 1/2X_0) + b_i(\mp 1/2X_\mp) + c_i(\mp 1/2X_\pm)$$

and apply to a monomer with parameters Δ_A and β_A. The matrix elements of the electric dipole operator are

$$\langle \Phi_{i\pm}{}^Z|P^Y|\Phi_{0\mp}\,Z\rangle = (-1)^{1/2}(c+d)[a_0(c_i+d_i) - (b_0+c_0)a_i]/(2)^{1/2}$$

$$\langle \Phi_{i\pm}{}^Z|P^X|\Phi_{0\mp}{}^Z\rangle = \pm(-c+d)[a_0(b_i-c_i) + a_i(c_0-b_0)]/(2)^{1/2}$$

$$\langle \Phi_{i\mp}{}^Z|P^Z|\Phi_{0\mp}{}^Z\rangle = a_0a_i(a-2b) + (b_ib_0+c_ic_0)(a+b) + (b_0c_i+c_0b_i)(-d)$$

Near-Infrared Absorption Spectra and MCD

The calculated energies, electric dipole intensities, and MCD intensities (in the linear limit) are given in Table IV for the parameters consistent with the g factors. The theory predicts that there should be electric dipole allowed transitions to three of the five possible states. The most intense of these lies highest in energy, and it should show a small MCD signal. There are two other, weaker, absorption bands, each showing larger MCD. The higher of these is assigned to a broad weak absorption identified by a relatively strong negative MCD which has been found in the Creutz–Taube ion at energies below that of the intense absorption at 6200 cm^{-1}. The negative MCD is very broad and extends beyond the lower limit of our apparatus (4000 cm^{-1}).[14]

Table IV. Calculated State Energies, Z-Polarized Dipole Strengths (D_{oZ}),[a] and MCD Spatially Averaged (Linear Limit) $\bar{C}_0$ Terms[b] for the Creutz–Taube Ion and the Osmium Analogue

Creutz–Taube ion			osmium analogue		
energy, cm^{-1}	D_{oZ}	$\bar{C}_o$	energy, cm^{-1}	D_{oZ}	$\bar{C}_o$
6170	0.762	0.033	11032	0.482	0.038
3201	0	0	6789	0	0
3167	0.014	−0.108	6760	0.003	−0.082
2171	0	0	4881	0	0
1834	0.224	0.075	3078	0.514	0.044

[a] In units of a^2. [b] In units of $a(c+d)g_X/[3(2)^{1/2}]$.

The relative phases of the electric dipole matrix elements are not determined by theory, and thus the signs calculated for the MCD intensities are also unknown. We thus can only be concerned with relative signs.

The strong polarization of the intense band has been experimentally established,[1] so the parameter $a(V(A_1))$ is most likely dominant in the intensity process. Thus the cross (interference) terms between electric dipole operators P^Z and P^X with $B//Y$ or P^Z and P^Y with $B//X$ must dominate the MCD of the allowed band. The observed signs of the MCD, + at 6200 cm^{-1} and − at lower energies, are consistent with $c \approx d$ when $A_X = 0$. The low intensity in X polarization has been determined experimentally[1] from single-crystal measurements of the tosylate salt.

Thus our model is able to rationalize the substantial MCD of the intense band and further accounts for the relatively strong MCD of opposite sign at lower energies. There are, however, some disturbing features indicating that a completely satisfactory analysis would have to include vibronic coupling. Perhaps the most serious difficulty is the prediction of the third absorption band at 1852 cm^{-1} with over 20% of the intensity of the intense band. There have been reports[1] of a band at ~2000 cm^{-1} apparently sample dependent but with much lower intensity.

A possible explanation lies in the observed (via MCD) extreme width of the 3200-cm^{-1} band. If the lower energy band were also very broad it could also escape detection by absorption measurements on pressed disks that do not allow the determination of accurate base lines. A measurement of the MCD in this region would be much more definitive as vibrational features have vanishing MCD, and the width of a band would not preclude the observation of a transition.

Furthermore, the MCD of the intense band does not follow the absorption profile.[14] This immediately indicates either structure within the electronic transition or vibronic activity. Involvement of a totally symmetric mode as suggested by Hush[15] would lead an MCD band shape identical with that observed in absorption. It is difficult to envisage further electronic states at the same energy as the t_2 manifold, which is well separated from other configurations, and overall we take this as evidence for vibronic activity in the system.

An application of our model to the absorption spectrum of the analagous osmium ion recently reported[16] is convincing. Spin-orbit coupling for Os^{3+} is very strong, and the interaction between the two ions is also stronger. This brings all the intensites and energies into a regime that is more easily observable. The combined

(13) Sugano, S.; Tanabe, Y.; Kamimura, H. "Multiplets of Transition-Metal Ions in Crystals"; Academic Press: New York, 1970; p 205.

(14) Krausz, E. R.; Ludi, A. *Inorg. Chem.*, in press.

(15) Hush, N. S. "Mixed Valence Compounds"; Brown, D. B., Ed.; Reidel: Dordrecht, 1980; p 151.

(16) Magnuson, R. H.; Lay, P. A.; Taube, H. *J. Am. Chem. Soc.* **1983**, *105*, 2507–2509.

influence of a stronger spin-orbit coupling and electronic interaction might reduce the chance of a fluctional or vibronic process occurring.

There are three absorption bands in the red and near-infrared region at 11 200, 6700, and 3000 cm^{-1}: the highest and lowest carry rougly equal intensity while the middle band is quite weak. Using the tetragonal and rhombic parameters obtained above from an analysis of the Creutz-Taube ion g factors as outlined above, plus a value of $W = 4600$ cm^{-1} and $\lambda = 3000$ cm^{-1}, we then calculate the energy levels and relative intensities given in Table IV. The agreement between calculated and observed band positions is very good, and the relative intensities of the bands are well accounted for. It remains to measure the MCD intensities and g values to complete the analysis. The significance of this fit is that the tetragonal and rhombic parameters are the same as those that account for the properties of the Creutz-Taube ion and are thus truly single-ion properties that are maintained when the ions are coupled. Our conclusion would be that the osmium analogue is definitely delocalized, but there are indications that there is substantial vibronic activity in the Creutz-Taube ion.

Acknowledgment. We acknowledge the help of Dr. R. J. Robbins in providing a computer routine to fit the g values with our model.

Registry No. Decaammine(μ-pyrazine-N,N')diruthenium(5+), 93503-78-7; decaammine(μ-pyrazine-N,N')diosmium(5+), 85282-23-1.

Resonance Raman Spectroscopy of Metallochlorins: Models for Green Heme Protein Prosthetic Groups

Laura A. Andersson,[†] Thomas M. Loehr,*[†] Chi K. Chang,[‡] and A. Grant Mauk[⊥]

Contribution from the Department of Chemical, Biological, and Environmental Sciences, Oregon Graduate Center, Beaverton, Oregon 97006, the Department of Chemistry, Michigan State University, East Lansing, Michigan 48824, and the Department of Biochemistry, University of British Columbia, Vancouver, BC V6T 1W5, Canada. *Received July 27, 1984*

Abstract: Iron chlorin complexes have been investigated by resonance Raman (RR) spectroscopy as models for the prosthetic groups of green heme proteins. Fe^{III}pPP (pPP = photoprotoporphyrin IX dimethyl ester) and Fe^{III}DC (DC = deuterochlorin IX dimethyl ester) complexes were examined with 406.7-, 457.9-, 488.0-, 514.5-, and 568.2-nm excitation lines in the high-frequency (>1000 cm^{-1}) spectral region. The general characteristics of the chlorin spectra have been analyzed and vibrational modes have been assigned in a comparative study with the analogous iron porphyrins, Fe^{III}PP (PP = protoporphyrin IX dimethyl ester) and Fe^{III}DP (DP = deuteroporphyrin IX). Although vibrational frequencies above 1000 cm^{-1} for the spectra of Fe^{III}DC and Fe^{III}pPP complexes were generally similar to those of the analogous porphyrins, major differences were observed in both patterns of relative intensity and in the depolarization ratios. For example, all B_{1g} (depolarized) porphyrin modes become totally symmetric (polarized) vibrational modes in chlorin spectra. At least six new bands are present in metallochlorin spectra. Of particular interest is the observation of new polarized "chlorin" bands flanking the oxidation state marker, ν_4. These findings reflect a dramatic reduction in molecular symmetry from an effective D_{4h} for metalloporphyrins to an effective $C_2(x)$ for metallochlorins. We also performed a comparative analysis of published M-OEC (OEC = octaethylchlorin) and M-OEP (OEP = octaethylporphyrin) RR spectra to verify that our observations were characteristic of metallochlorins in general. In every case, the M-OEC complexes exhibit RR spectra with a greater number of bands, a new polarized feature in the region of the oxidation-state marker, and a striking increase in the number of polarized Raman bands. In addition, we have found that many characteristic metalloporphyrin vibrational frequencies and assignments, such as for oxidation and spin-state markers and peripheral substituents (i.e., vinyl or carbonyl), are transferable to the study of metallochlorin complexes. Clearly these observations have predictive value and establish testable criteria for identification of metallochlorin prosthetic groups in biological systems such as the green heme proteins.

Heme proteins and heme enzymes are ubiquitous biological molecules involved in oxygen transport and oxygen metabolism. Whereas in heme systems chemical control is generally manifested by variations in axial ligation and the nature of the heme environment, reduction of the porphyrin macrocycle provides an alternate means whereby the reactivity of these macromolecules may be expressed. Examples of such partially saturated systems includes dihydroporphyrins, or chlorins; tetrahydroporphyrins, or sirohemes; and the highly reduced macrocycles of vitamin B-12 and cofactor F-430. Metallochlorin complexes, which are the subject of this investigation, occur in chlorophyll pigments and at the active sites of some members of a newly recognized class of proteins known as the green heme proteins. Work in this and other laboratories suggests that the chlorin prosthetic group is found in sulfmyoglobin[1-3] and sulfhemoglobin (a major nonfunctional form of human hemoglobin),[2b] hemes d and d_1 of microorganisms,[4] *Neurospora crassa* catalase,[5] leukocyte myeloperoxidase,[3,6,7] and bovine spleen green heme protein.[3,7] Although a metallochlorin prosthetic group has been implicated for each of these proteins, the exact macrocyclic ring modification(s) and site of ring reduction are still not completely known in most

[†] Oregon Graduate Center.
[‡] Michigan State University.
[⊥] University of British Columbia.

(1) Morell, D. B.; Chang, Y. Clezy, P. S. *Biochim. Biophys. Acta* **1967**, *136*, 121-136.
(2) (a) Peisach, J.; Blumberg, W. E.; Adler, A. *Ann. N.Y. Acad. Sci.* **1973**, *206*, 310-327. (b) Berzofsky, J. A.; Peisach, J.; Blumberg, W. E. *J. Biol. Chem.* **1971**, *246*, 3367-3377.
(3) Andersson, L. A.; Loehr, T. M.; Lim, A. R.; Mauk, A. G. *J. Biol. Chem.*, in press.
(4) Lemberg, R.; Barrett, J. "Cytochromes"; Academic Press: London, 1973; pp 233-245.
(5) (a) Jacob, G. S.; Orme-Johnson, W. H. *Biochemistry* **1979**, *18*, 2967-2975. (b) Jacob, G. S.; Orme-Johnson, W. H. *Biochemistry* **1979**, *18*, 2975-2980.
(6) Sibbett, S. S.; Hurst, J. K. *Biochemistry* **1984**, *23*, 3007-3013.
(7) Babcock, G. T.; Ingle, R. T.; Oertling, W. A.; Davis, J. S.; Averill, B. A.; Hulse, C. L.; Stufkens, D. J.; Bolscher, B. G. J. M.; Wever, R. *Biochim. Biophys. Acta*, in press.

0002-7863/85/1507-0182$01.50/0